International Journal of Bioprinting

RESEARCH ARTICLE

Effect of ionic crosslinking on morphology and thermostability of biomimetic supercritical fluids-decellularized dermal-based composite bioscaffolds for bioprinting applications

Run-Miao Yang[1,2†], Jun Xu[2,3,4†], Ching-Cheng Huang[5,6*]

[1]Department of Material Engineering, Jiangsu University of Technology, Chang Zhou, Jiangsu, China

[2]PARSD Biomedical Material Research Center (Chang Zhou), Chang Zhou, Jiangsu, China

[3]College of Food Science and Engineering, Hainan University; Engineering Research Center of Utilization of Tropical Polysaccharide Resources, Ministry of Education, Haikou 570 228, Hainan, China

[4]State Key Laboratory of Biochemical Engineering, Institute of Process Engineering, CAS 100 190, Beijing, China

[5]Department of Biomedical Engineering, Ming-Chuan University, Taoyuan 320-33, Taiwan

[6]PARSD Biomedical Material Research Center (Taiwan), Taichung, Taiwan

[†]These authors contributed equally to this work.

***Corresponding author:**
Ching-Cheng Huang
(junas.tw@yahoo.com.tw)

Citation: Yang R, Xu J, Huang C, 2023, Effect of Ionic crosslinking on morphology and thermostability of biomimetic supercritical fluids-decellularized dermal-based composite bioscaffolds for bioprinting applications. *Int J Bioprint,* 9(1): 625.

http://doi.org/10.18063/ijb.v9i1.625

Received: April 27, 2022;

Accepted: August 11, 2022;

Published Online: October 27, 2022

Abstract

In the present study, supercritical fluid was employed to prepare a kind of supercritical fluids-decellularized dermal-based scaffold (SFDDS) from porcine dermal tissue. Further, new composite bioscaffolds containing SFDDS were designed for bioprinting applications. Then, the effect of crosslinking functionality on microstructures and thermal properties of the composite bioscaffolds containing decellularized extracellular matrix were studied. The results of thermal stability from thermogravimetric analysis and difference thermogravimetry demonstrated the structural stability of the composite bioscaffolds. A method was designed to prepare bioinspired decellularized dermal-based composite bioscaffolds, which were further characterized by infrared spectroscopy, scanning electron microscopy, and thermogravimetry analysis.

Keywords: Alginate; Composite membrane; Decellularization; Microstructure; Supercritical carbon dioxide

1. Introduction

Numerous natural or modified materials with specific microstructures have been studied for medical or bioprinting applications, for instance, the application of bioinks or bioscaffolds for tissue reconstruction[1-8]. A wide range of materials with varied viscosities and high cell density aggregates can be 3D printed using this technique[2]. A large variety of polymers is under research for the use in bioprinting technology. Natural polymers, including collagen[3], gelatin[4], alginate[5], and hyaluronic acid[6], and synthetic polymers, such as polyvinyl alcohol (PVA)[7] and polyethylene glycol, are commonly used in bioinks for 3D printing. Often, these bioinks are post-processed

either by chemical or ultraviolet (UV) crosslinking to enhance the mechanical properties of the constructs. Depending on the type of polymer used in the bioink, biological tissues and scaffolds of varied complexity can be fabricated[2]. Alginate is a natural polysaccharide that typically originates from various species of algae. Due to its low cost, good biocompatibility, and rapid ionic gelation, the alginate hydrogel is a good option of bioink source for 3D bioprinting. However, the lack of cell adhesive moieties was the critical limitation of alginate hydrogel bioink[8].

For natural material, collagen is the most abundant protein in animals and has been widely used in the biomedical applications as a biomaterial[9]. Decellularized matrix containing collagen segments is considered a desirable bioscaffold for tissue regeneration because the decellularized matrix maintains the original components of native tissue, which could constitute the main structural element to provide biocompatibility, structural stability, physical and structural configuration, cell adhesion, and cell migration for direct tissue development in bioprinting applications[10,11]. The decellularized bioscaffold could be obtained and purified by a combined procedure with decellularizing and defatting, such as supercritical fluid treatments, chemical treatments, and enzyme treatments[12]. Supercritical fluids could extract the fat without damaging and affecting the collagen segments. Furthermore, the supercritical fluids could be employed at a critical temperature of 31°C, which was low enough for processing collagen. Supercritical fluids could provide a good and clean choice for decellularizing and defatting procedures which have outstanding properties, such as being non-corrosive, non-toxic, and non-flammable property[13-15]. For natural material, sodium alginate, which was extracted from marine brown algae[16,17], has a wide range of biomedical and bioprinting applications, such as cell immobilization and tissue regeneration[18-20].

Extrusion-based three-dimensional (3D) bioprinting strategies are widely used for producing 3D tissue constructs. This technology has rapidly evolved over the past two decades, providing a powerful tool set for the biofabrication of tissues that can facilitate translational efforts in the field[21]. Several studies have been conducted to explore suitability of extrusion bioprinting in the aspects of rheological property, printability and biocompatibility, which could provide many valuable information for bioprinting application[21]. Further, computer-aided processes have been studied and used to build up new 3D bioprinting strategies, which would play an important role for 3D bioprinting application[22].

In this study, a new biomimetic decellularized dermal-based bioscaffold for extrusion bioprinting was designed and prepared. The bioscaffold was applied to design a series of composite bioscaffolds for bioprinting applications. Furthermore, the morphology, structural stability, and thermostability of the resulting biomimetic supercritical fluids-decellularized dermal-based composite bioscaffolds were studied to provide another valuable view for bioprinting applications. Supercritical carbon dioxide ($ScCO_2$) was employed to prepare a kind of supercritical fluids-decellularized dermal-based bioscaffold (SFDDS). In the previous works, supercritical fluid-based decellularization protocols were shown to have great advantage over the conventional decellularization as it may allow preservation of extracellular matrix components and structures[1]. The $ScCO_2$ decellularization would significantly reduce treatment times, achieve complete decellularization, and preserve extracellular matrix structure. The rupture of the cells as a result of high pressure of the fluid during the treatment and rapid depressurization is expected to be effective in removing the cells from the tissues[1]. The resulting SFDDS was introduced into the alginate-based bioink. A series of new alginate-based composite bioscaffolds containing SFDDS were designed and obtained. The new design of composite bioscaffolds has high stability and excellent biological properties of the scaffolds in orthopedics and gene therapy. The composite bioscaffolds containing collagen scaffolds were characterized by Fourier transform infrared (FTIR), scanning electron microscopy (SEM), and thermogravimetric analysis (TGA) to obtain the results on thermostabilities and morphology. Effect of ionic crosslinking reaction with various crosslinking time on structural stability and thermal stability of the resulting composite bioscaffolds was further studied.

2. Materials and methods

2.1. Materials

Chemicals utilized in the present study include sodium alginate (Sigma-Aldrich Company), sodium hydroxide (Sigma-Aldrich Company), Triton X-100 (Sigma-Aldrich Company), calcium chloride ($CaCl_2$, Fluka Company), 0.5M acetic acid, 20% alcohol, sodium dihydrogen phosphate, and disodium hydrogen phosphate (First Chemical Works Company).

2.2. Preparation of SFDDS

Before enzyme treatment being used for removing most fatty acids and tissues of raw porcine dermal, the $ScCO_2$ was employed to prepare a new scaffold at 45°C and 18 mPa for 6 h. Furthermore, raw porcine dermal samples were treated at 25°C by aqueous sodium hydroxide solution (2 wt %) for 2 h and followed by aqueous Triton X-100

solution (3 wt %) for 2 h. The resulting supercritical fluids-decellularized dermal-based sample was washed with double-distilled water under ultrasonic wave, frozen for 6 h, and then lyophilized (EYELA and FD-5N) at −45°C and 0.1 – 0.2 torr. A kind of SFDDS was obtained[23].

2.3. Preparation of alginate-based composite bioscaffolds containing ALG and SFDDS

First, the desired amount of SFDDS bioscaffold was added and dispersed completely in 40 mL of double-distilled water to obtain dispersed SFDDS solution. Then, aqueous sodium alginate solution was homogenized thoroughly with the dispersed SFDDS solution at 26,000 rpm for 3 min to obtain an aqueous ALG/SFDDS solution. Further, the resulting aqueous ALG/SFDDS solution was molded and lyophilized at a freeze-drying temperature of −45°C and pressure of 0.1 – 0.2 torr overnight. A series of alginate-based composite bioscaffolds with SFDDS bioscaffolds were obtained based on the various ratios of sodium alginate and SFDDS (ALG/SFDDS: 80/20, 85/15, and 90/10; w/w) (Table 1 and Figure 1)[15,24].

2.4. Preparation of cross-linked alginate-based composite bioscaffolds

The alginate-based composite bioscaffold containing ALG and SFDDS was cross-linked in aqueous $CaCl_2$ solution at different crosslinking times such as 2, 4, 6, 8, and 10 min. The cross-linked ALG/SFDDS was then frozen and dried. The cross-linked alginate-based composite bioscaffolds with supercritical fluids-decellularized dermal-based collagen bioscaffold could be obtained (Table 1 and Figure 1).

Table 1. Preparation of ionic cross-linked composite bioscaffolds with SFDDS.

Sample no.	ALG/SFDDS[a] (w/w)	Ionic crosslinking time[b] (min)
ADDS0T1	100/0	2
ADDS0T5	100/0	10
ADDS1T1	90/10	2
ADDS1T2	90/10	4
ADDS1T3	90/10	6
ADDS1T4	90/10	8
ADDS1T5	90/10	10
ADDS2T1	85/15	2
ADDS2T5	85/15	10
ADDS3T0	80/20	0
ADDS3T1	80/20	2
ADDS3T5	80/20	10

[a]ALG: Alginate; SFDDS: Decellularized dermal scaffold through $ScCO_2$ treatment.
[b]The reaction time for ionic crosslinking reaction with 0.5 wt% $CaCl_2$ (aq).

2.5. Instruments

FTIR was determined with a spectrometer (Nicolet IS10, Thermo Fisher Scientific, USA), and the data were collected from 400 to 4000 cm^{-1}. Morphology was studied by SEM (S3400N, Hitachi, Japan). Thermal analysis was performed by TGA using a thermoanalyzer (7300TG/DTA, Seiko, Japan).

3. Results and discussion

In this study, the SFDDS was prepared and identified by collagen. The $ScCO_2$ decellularization significantly reduced treatment times, achieved complete decellularization, and

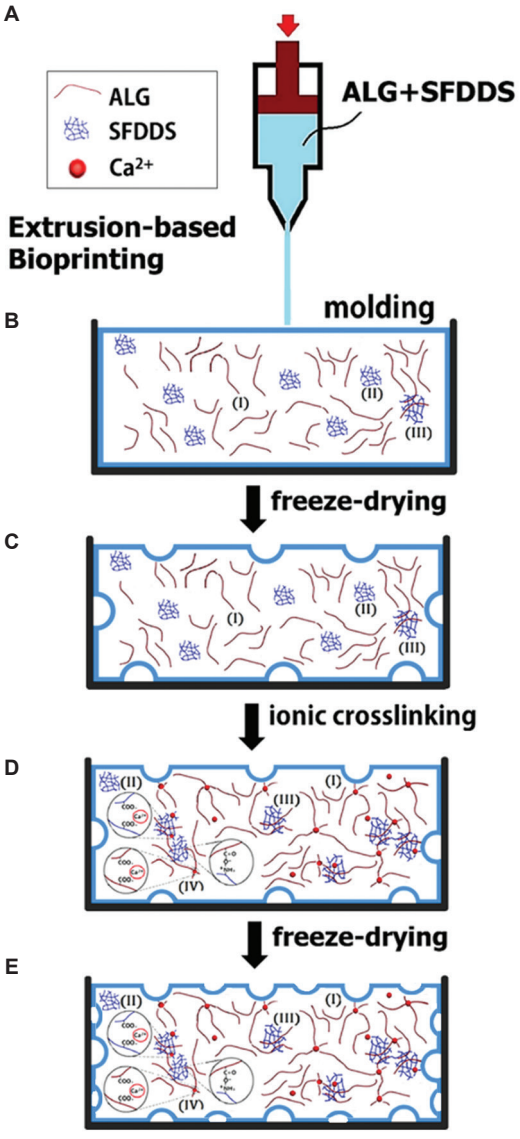

Figure 1. Schematic drawing for preparation of ionic cross-linked composite bioscaffold was illustrated, including (A) extrusion-based bioprinting procedure, (B) molding procedure, (C) freeze-drying, (D ionic crosslinking procedure, and (E) freeze-drying procedure.

preserved extracellular matrix structure. High pressure of the fluid could rupture the cells during the treatment and rapid depressurization[1]. A series of alginate-based composite bioscaffolds with different introducing amounts of SFDDS were prepared by lyophilization. Further, the resulting alginate-based composite bioscaffolds were cross-linked with aqueous $CaCl_2$ to prepare the corresponding ionic cross-linked composite bioscaffolds with enhanced structural stability and thermal stability. The morphology and thermal stability with various ionic crosslinking time were studied, the composite bioscaffolds were sampling every 2 min from 2 min to 10 min as listed in Table 1. Possibly, the crosslinking functionality would affect the microstructures of cross-linked composite bioscaffolds during various ionic crosslinking times. Depending on different ionic crosslinking time, the Ca^{2+} ions might penetrate inside the loose microstructures with rich porosity. The penetrated Ca^{2+} ions would be associated with acidic groups within composite bioscaffolds.

3.1. Identification of alginate-based composite bioscaffolds

From the results of FTIR spectroscopy, the alginate-based composite bioscaffolds containing decellularized SFDDS were identified through collagen characterization. The incorporation of SFDDS in the resulting alginate-based composite bioscaffolds was confirmed.

From the spectra of SFDDS, the amide A band and B band were centered at 3289 and 3182 cm^{-1}, respectively, which were attributed to the stretching vibration of N-H group. In addition, the absorption bands at 1632 cm^{-1} and 1552 cm^{-1} were attributed to amide I and amide II of collagen structures, respectively. The absorption band at 1454, 1408, 1336, and 1241 cm^{-1} was attributed to the amides III of collagen structures (Figure 2A). The amide I band is related to the stretching vibrations of C=O groups, which participate in the formation and maintenance of the triple helical structure of collagen. The amide II band was related to N–H bending and C–N stretching vibrations, which generally occur in the 1550 – 1600 cm^{-1} range. A shift to lower wavenumbers would be observed when it participates in the formation of hydrogen bonds. Amide III was related to C–N stretching vibration and N–H deformation[25-28]. For ADDS3T0, absorption bands of the -COOH group and NH_2 group in comparison with the pure components are shown in Figure 2. Due to the strong absorption of collagen, the signal differences of COOH group and NH_2 group were overlapped with absorption band of SFDDS (Figure 2B). The FTIR spectra of alginate are shown in Figure 2C, and typical absorption bands were observed, such as the band at 3338 cm^{-1} for O–H stretching, the bands at 2901 and 2921 cm^{-1} for C–H stretching of pyranoid ring, the band at 1590 cm^{-1} for COO symmetric stretching, the band at 1410 cm^{-1} for COO asymmetric stretching, the band at 1296 cm^{-1} for C–O stretching, and the bands at 1072 cm^{-1} and 1002 cm^{-1} for C–O–C stretching.

In the spectra of the resulting alginate-based composite bioscaffolds with ALG and SFDDS, such as ADDS3T5 (Figure 2D), besides retaining the above-mentioned bands of alginate, such as the pyranoid ring (6-membered ring) C–H stretching at 2920 cm^{-1} and 2851 cm^{-1}, COO symmetric stretching at 1605 cm^{-1}, COO asymmetric stretching at 1409 cm^{-1}, C–O stretching at 1296 cm^{-1}, and C–O–C stretching at 1082 cm^{-1} and 1022 cm^{-1}, the absorption bands at 1605 cm^{-1} for the carbonyl group and 1537 cm^{-1} for asymmetric and symmetric stretching of carboxylate salt groups were also observed. A strong absorption band at 1605 cm^{-1} and two remarkably shoulders at 1610 cm^{-1} and 1550 cm^{-1} were attributed to carbonyl groups of SFDDS. In the spectra of resulting alginate-based composite bioscaffold, such as ADDS3T5,

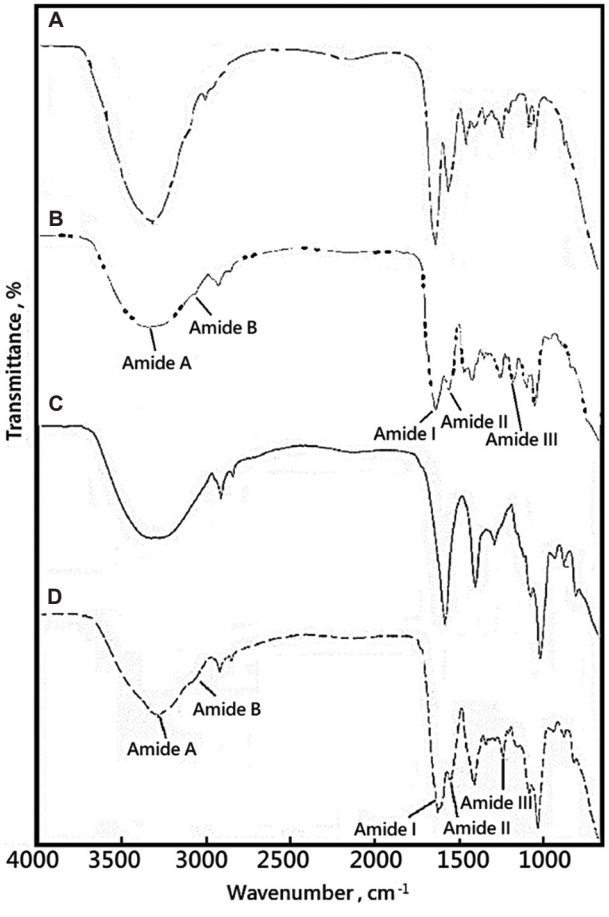

Figure 2. FTIR results of (A) SFDDS, (B) ADDS3T0, (C) ALG, and (D) cross-linked alginate-based composite bioscaffold of ADDS3T5.

the absorption bands at 3293 and 3120 cm^{-1} were attributed to the N-H stretching vibration of amide A and amide B, respectively (Figure 2D). The amide A of the spectrum had direct relationships with changes in collagen triple helix and hydrogen bonding patterns. The absorption peak at 3293 cm^{-1} of ADDS3T5 was the amide A band, which is due to N–H stretching vibration and hydrogen bonds. When N–H participates in the formation of a hydrogen bond, the wavenumber of its stretching vibration would be shifted to ~3300 cm^{-1}[25-28]. The amide B band was related to asymmetric stretch vibrations of $–NH_3^+$ and =C–H, and the shift of amide B to higher wavenumber (~3120 cm^{-1}) was associated with an increase in free $NH–NH_3^+$ groups from both lysine residues and the N-terminus[25-28]. The same results were observed in ADDS1T5, ADDS2T5, and ADDS3T5.

3.2. Morphology of alginate-based composite bioscaffolds with decellularized SFDDS

The microstructures of cross-linked ALG bioscaffolds, such as ADDS0T1 and ADDS0T5 (Table 1), were characterized by SEM (Figure 3). The sheet shape loose bioscaffold could be found. Furthermore, SEM results of new alginate-based composite bioscaffolds with decellularized SFDDS bioscaffolds are shown in Figures 3-5. Effect of ionic crosslinking on morphology of designed composite bioscaffolds with different introducing amounts of SFDDS was studied. The remarkable porous microstructures could be exhibited in the alginate-based composite bioscaffolds. With the increasing introducing amounts of SFDDS, the porous microstructure could be changed to a relatively compacted microstructure. It might be due to the crosslinking reaction that enhanced the compacted microstructures of alginate-based composite bioscaffolds. The high introducing amount of SFDDS would provide a relative complicated microenvironment in existence of slight $CaCl_2$ (0.5 wt%), as illustrated in Figure 6.

When a little amount of SFDDS was introduced into the alginate-based composite bioscaffolds with 0.5 wt% $CaCl_2$ during different ionic crosslinking time, weak association between functional groups would be formed, such as weak ionic interactions among Ca^{2+} ions and acidic groups of ALG and weak interaction between ammonium group of SFDDS and acidic group of ALG, as shown in Figure 2. Most

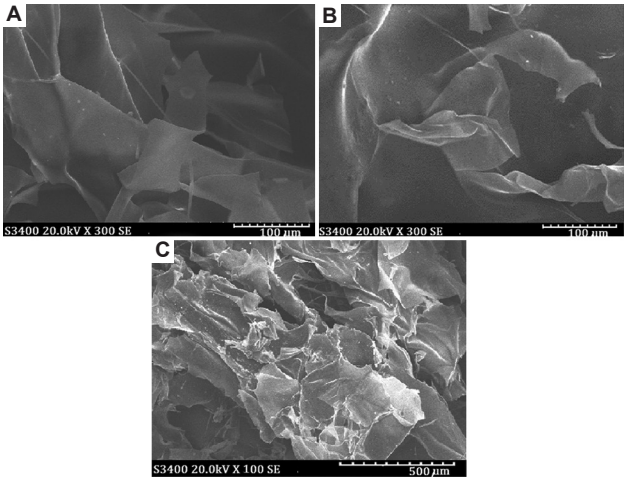

Figure 3. Morphology of the alginate-based bioscaffolds. (A) ADDS0T1 (300×), (B) ADDS0T5 (300×), and (C) ADDS0T5 (100×).

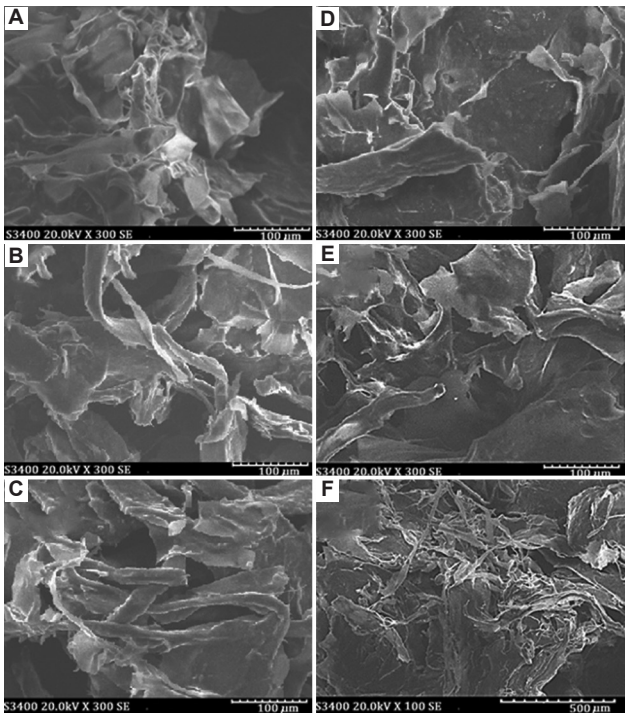

Figure 4. Morphology of the alginate-based composite bioscaffolds. (A) ADDS1T1 (300×), (B) ADDS1T2 (300×), (C) ADDS1T3 (300×), (D ADDS1T4 (300×), (E) ADDS1T5 (300×), and (F) ADDS1T5 (100×).

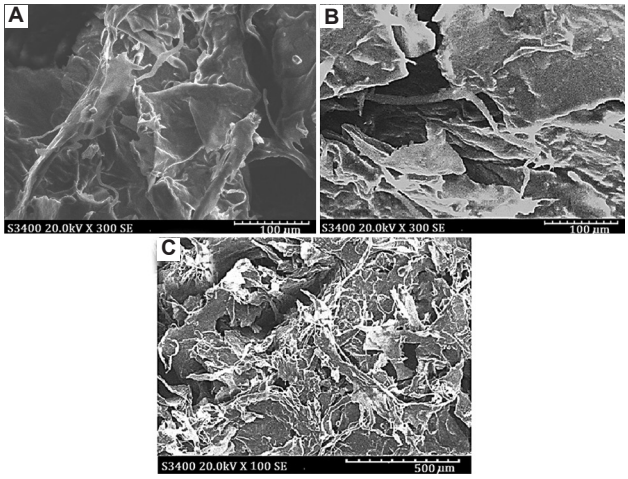

Figure 5. Morphology of the alginate-based composite bioscaffolds. (A) ADDS2T1 (300×), (B) ADDS2T5 (300×), and (C) ADDS2T5 (100×).

area of alginate-based composite bioscaffolds exhibited a sheet shape microstructure similar to that for alginate bioscaffold. The degree of sheet shape microstructure would increase with ionic crosslinking time as shown in Figures 4A and B. Some area of composite bioscaffolds would show a mixed shape containing block shape and fibrous shape in the microstructure, which might be due to the mixed association among ALG segments and SFDDS segments (Figure 4B-F).

When a large amount of SFDDS was introduced into the alginate-based composite bioscaffolds with 0.5 wt% $CaCl_2$, some interactions would build up a complicated microstructure, as shown in Figure 6. These interactions would contribute to ionic interaction between acidic group of ALG and ammonium group of SFDDS, ionic interaction among Ca^{2+} ions, acidic groups of ALG molecules, and acidic groups of SFDDS, and ionic interaction between Ca^{2+} ions and acidic groups of SFDDS. Most area of composite bioscaffolds would show a block shape in the microstructure, which might be due to the mixed interaction among ALG and SFDDS in the existence of Ca^{2+} ions, such as ADDS1T5, ADDS2T5, and AddS3T5, as shown in Figures 4E, 4F, 5B, 5C, 6B, and 6C. As the incorporation of SFDDS increasing, the fibrous shape and block shape microstructure would be increased. In the morphology of ADDS3T5, a relative remarkable block shape microstructure in comparison with ADDS2T5 was observed which would be contributed to the complicated microstructure. Before penetration of Ca^{2+} ions, the non-ionic crosslinking structure containing microstructures (I), (II), and (III) was formed (Figure 7A). When the soaking time increased, penetration of Ca^{2+} ions would be increased to form weak ionic crosslinking structure containing microstructures (I), (II), and (III) (Figure 7B).

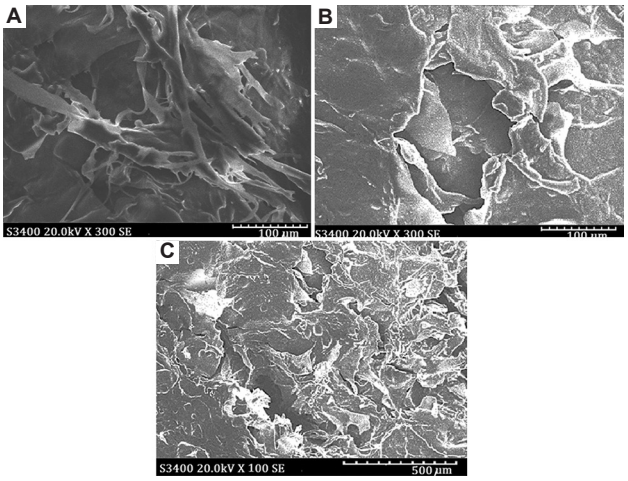

Figure 6. Morphology of the alginate-based composite bioscaffolds. (A) ADDS3T1 (300×), (B) ADDS3T5 (300×), and (C) ADDS3T5 (100×).

The penetration of Ca^{2+} ions would be increased with soaking time. After a relative long soaking time, a large amount of Ca^{2+} ion would penetrate into the microstructure of the alginate-based composite bioscaffolds with SFDDS to form a strong ionic crosslinking structure containing microstructures (I), (II), (III), and (IV) (Figure 7C).

3.3. Structural stability and thermal stability of alginate-based composite bioscaffolds with decellularized SFDDS

Effect of Ca^{2+} ion penetration on structural stability and thermal stability of alginate-based composite bioscaffolds containing decellularized SFDDS was discussed. TGA and difference thermogravimetry (DTG) results were employed to study the structural stability and thermal

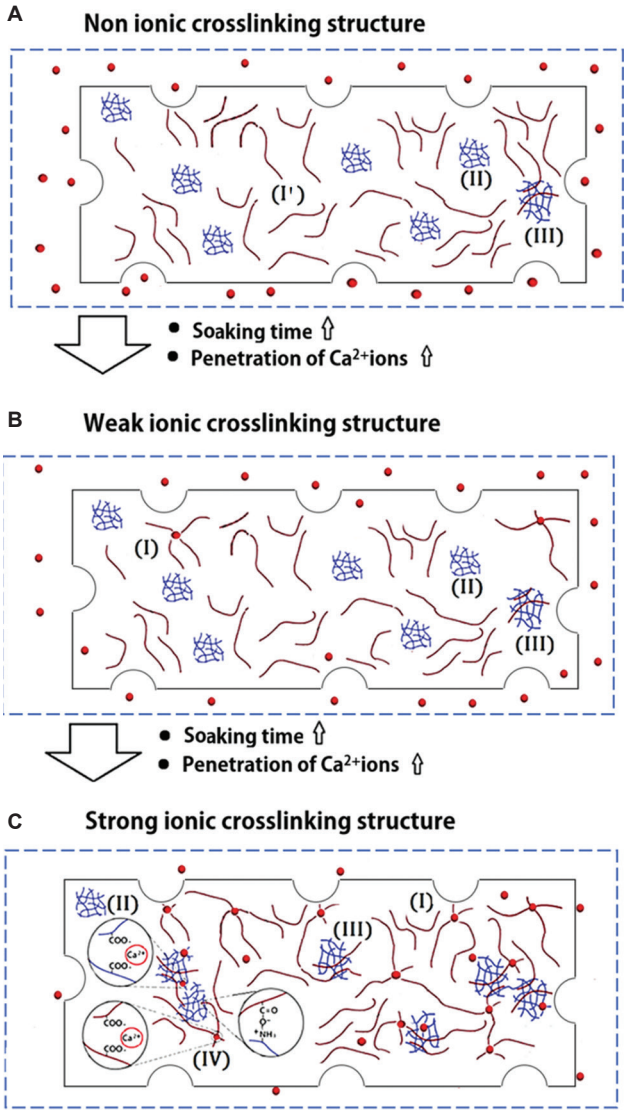

Figure 7. (A) Non-ionic crosslinking structure, (B) weak ionic crosslinking structure, and (C) strong ionic crosslinking structure.

stability of alginate-based composite bioscaffolds with SFDDS (Figure 8). The maximum pyrolysis temperature (T_{dMax}) of the alginate was ca. 250°C. In this study, the supercritical fluids-decellularized dermal-based bioscaffold (SFDDS) that was used to prepare alginate-based composite bioscaffolds might have relatively high thermal stability and good structural stability. The T_{dmax} of the alginate-based composite bioscaffolds was higher than 300°C, indicating that the bioscaffolds become heat-resistant biomaterial, following the introduction of SFDDS molecules after a suitable crosslinking reaction (e.g., soaking time > 5 min), which is suitable for bioprinting applications (Figure 8C-E). If the soaking time is too short,

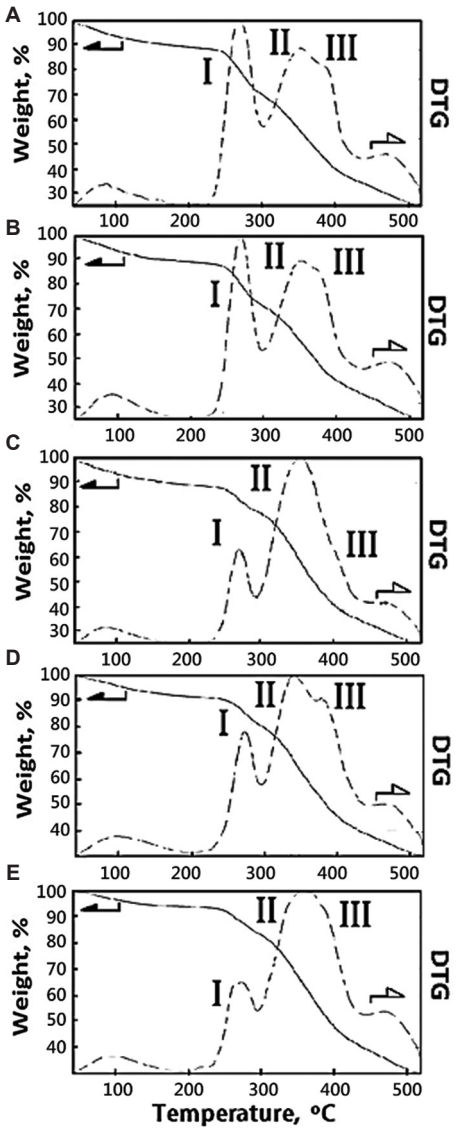

Figure 8. TGA and DTG results of alginate-based composite bioscaffolds: (A) ADDS1T1, (B) ADDS1T2, (C) ADDS1T3, (D) ADDS1T4, and (E) ADDS1T5.

the T_{dmax} of the alginate-based composite bioscaffolds exhibited a temperature lower than 300°C, which would be due to the non-ionic cross-linked structure and weak cross-linked structure (Figures 7A, B and 8A, B). DTG curves would provide useful information to study the effect of Ca^{2+} ion penetration on structural stability and thermal stability. Different microstructures, such as (I), (II),(III), and (IV) (Figure 7A and B), might be proposed depending on the TGA and DTG results, which exhibited maximum pyrolysis temperatures in different temperature stages, such as the T_{dmax} peak of ca. 90°C at the stage of 50 – 200°C, the T_{dmax} peak of ca. 270°C at the stage of 200 – 300°C, the T_{dmax} peak of ca. 360°C at the stage of 300 – 400°C, and the T_{dmax} peak of ca. 460°C at the stage of 400 – 500°C. Formations of specific microstructures would be reflected in T_{dmax} peaks of DTG curves. Before ionic crosslinking reaction, a series of porous alginate-based composite bioscaffolds could be lyophilized and obtained. Furthermore, the resulting alginate-based composite bioscaffolds were ionically cross-linked with $CaCl_2$ (aq) to obtain cross-linked alginate-based composite bioscaffolds through Ca^{2+} ion penetration. The Ca^{2+} ions could penetrate into the porous microstructures during the different soaking time. The Ca^{2+} ions could not penetrate into the porous microstructures completely during the short soaking time (Figure 7A). Most of microstructures would be proposed as microstructure I and microstructure II. The microstructure III might be formed with the increase of soaking time in an aqueous solution of $CaCl_2$. The heat resistance would be enhanced.

The T_{dmax} of cross-linked composite bioscaffolds was lower than 400°C. Even most of ALG molecules could be associated with SFDDS, as shown in Figure 8D and E. Compared with SFDDS, cross-linked composite bioscaffolds showed relatively high T_{dmax} of 360 – 380°C because of the formation of microstructure II and microstructure III (380°C). The T_{dmax} of SFDDS was observed at 340°C (Figure 9A). The increased T_{dmax} might be resulted from enhanced interaction among SFDDS and ALG segments. Compared with alginate-based ALG bioscaffold, the T_{dmax} of ALG molecules was observed at 240°C (Figure 9B). The cross-linked alginate-based composite bioscaffolds showed relatively high T_{dmax} of 270 – 280°C for microstructure I. The microstructure I could be regarded as cross-linked ALG molecules with Ca^{2+} ions.

New microstructures IV were formed and observed as shown in DTG results of Figure 9D and E when an increased amount of SFDDS was buried into alginate-based composite bioscaffolds with 0.5 wt% $CaCl_2$. T_{dmax} of cross-linked composite bioscaffolds, which was relatively higher than 400°C, was observed, as shown in Figure 9C-E.

Even most of ALG molecules could be associated with SFDDS molecule, as shown in Figure 8D and E. A high ratio of introducing amounts of SFDDS and ALG such as 80/20 (PCM3T5) would provide a relatively complicated microenvironment in the existence of $CaCl_2$, which could introduce a complicated microstructure (microstructure III) within the cross-linked composite bioscaffolds (Figure 7).

TGA analysis of the composite bioscaffolds was performed. Main losses were observed in several temperature ranges such as 200 – 300°C, 300 – 400°C, and 400 – 500°C. The weight loss of TGA curve in temperature range of 50 – 200°C was due to the chemical and physisorbed water, which exhibited the weight loss of 5 – 12 wt%. The following main losses observed in the temperature ranges of 200 – 300°C, 300 – 400°C, and 400 – 500°C in the TGA and DTG results contributed to the combustion of the cross-linked alginate-based composite bioscaffolds for ALG segment, SFDDS segment, and associated microstructure. The corresponding T_{dmax} in different temperature ranges was observed at 280°C, 350°C, and 420°C. The cross-linked alginate-based composite bioscaffolds showed a good thermal stability compared with the porous alginate materials. The morphology and thermal stability with various ionic crosslinking time were studied, and the composite bioscaffolds were sampled every 2 min. After 10 min, the additional changes of morphology and thermal stability were not observed (230 – 240°C).

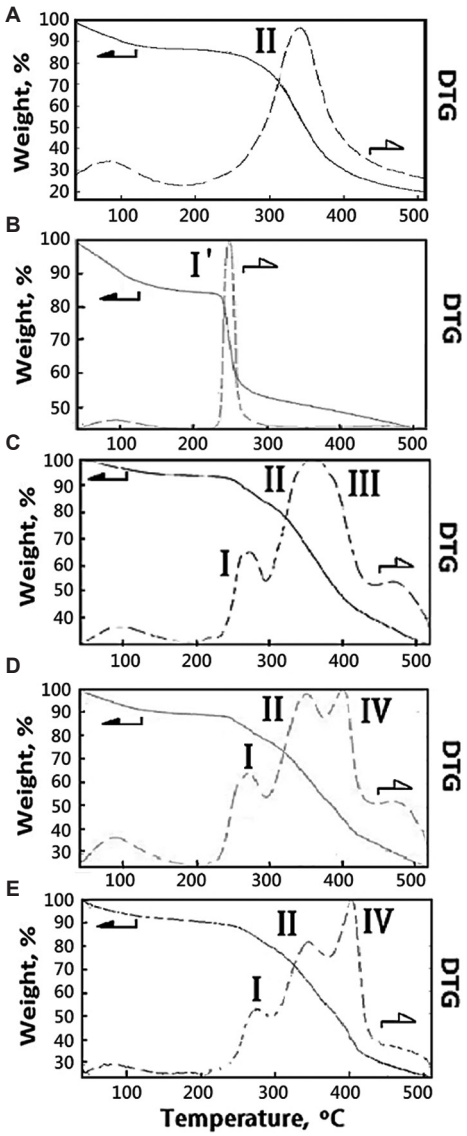

Figure 9. Thermogravimetric analysis of the alginate-based composite bioscaffolds: (A) SFDDS, (B) ALG, (C) ADDS1T5, (D) ADDS2T5, and (E) ADDS3T5.

3.4 Mechanical features of resulting cross-linked alginate-based composite bioscaffolds using extrusion-based bioprinting and freeze-drying procedures

The mechanical properties of the cross-linked alginate-based composite bioscaffolds, such as ADDS0T5, ADDS1T5, ADDS2T5, and ADDS3T5, using extrusion-based bioprinting and freeze-drying procedures were measured by tensile tests. Figure 10 shows the tensile strength and elongation at break. The cross-linked alginate-based composite bioscaffolds containing SFDDS (such as ADDS3T5) showed relatively better mechanical properties than the cross-linked alginate-based composite bioscaffolds without SFDDS (such as ADDS0T5). The introduction of decellularized SFDDS into the composite bioscaffolds enhanced mechanical properties. The tensile strengths of the cross-linked composite bioscaffolds were determined to be 6.3 mPa, 8.1 mPa, and 9.2 mPa for ADDS1T5, ADDS2T5, and ADDS3T5, respectively, which were relative higher than the value of 3.9 mPa for the composite bioscaffolds without SFDDS such as ADDS0T5, as shown in Figure 10.

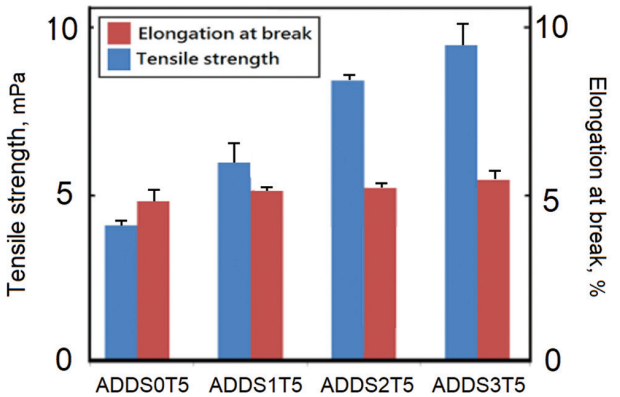

Figure 10. Tensile strength and elongation at break of alginate-based composite bioscaffolds: (A) ADDS0T5, (B) ADDS1T5, (C) ADDS2T5, and (D) ADDS3T5 (n = 3).

The elongation at break of the cross-linked alginate-based composite bioscaffolds showed almost the similar values in a range of 5.0 – 5.2%.

Introduction of decellularized extracellular matrix derived from porcine tissue into the materials showed relatively good mechanical properties and good thermal stability, which could be employed for biomedical applications using bioprinting technology and designing bioinks containing ALG and SFDDS with ALG/SFDDS in the ratio of 90/10 – 80/20. Furthermore, the cells might be introduced in the bioinks for tissue engineering applications. Naghieh *et al.* reported that the mechanical behavior of 3D-printed alginate scaffolds and the important printing parameters, such as printing speed, printing pressure, or material inflow, were the essential information in extrusion bioprinting for the preparation of 3D-printed macroscaffolds[29]. In this study, the 3D-printed scaffolds containing micro-bioscaffolds were considered and designed. The supercritical fluids-decellularization technique was applied to obtain decellularized dermal-based micro-bioscaffolds. The designed 3D-printed scaffolds containing supercritical fluids-decellularized dermal-based micro-bioscaffolds were successfully prepared by extrusion bioprinting and freeze-drying. For specific medical applications of 3D-printed macro-scaffolds containing the resulting micro-bioscaffolds in the future, the printing parameters for the preparation of 3D-printed macro-scaffolds might be useful to obtain preferable 3D-printed scaffolds[29].

4. Conclusions

A new cross-linked alginate-based composite bioscaffold containing supercritical fluids-decellularized dermal-based bioscaffolds, which could maintain the microstructure of integrity extracellular matrix, was successfully prepared. Effect of Ca^{2+} ion penetration on structural stability and thermal stability of the resulting cross-linked alginate-based composite bioscaffold was studied with different ionic crosslinking. Furthermore, several types of microstructures were proposed within the cross-linked alginate-based composite bioscaffolds in evidence of DTG and morphology results. The cross-linked alginate-based composite bioscaffolds exhibited good thermal stability, and its T_{dmax} could reach up to 400°C. Furthermore, the cross-linked alginate-based composite bioscaffolds showed a relatively good structural stability, indicating that it could be a potential biomaterial for bioprinting applications.

Acknowledgments

Authors would like to acknowledge the Taiwan PARSD Pharmaceutical Technology Consultants Ltd. Company for technical support.

Funding

None.

Conflict of interest

The authors declare no potential conflicts of interest with respect to the research, authorship, and/or publication of this article.

Author contributions

Supervision: Ching-Cheng Huang
Conceptualization: Ching-Cheng Huang
Investigation: Jun Xu
Formal analysis: Jun Xu
Writing – original draft: Run-Miao Yang
Writing – review & editing: Ching-Cheng Huang

Ethics approval and consent to participate

Not applicable.

Consent for publication

Not applicable.

Availability of data

The original contributions presented in the study are included in the article, and further inquiries can be directed to the corresponding author.

References

1. Huang CC, Chen YJ, Liu HW, 2021, Characterization of composite nano-bioscaffolds based on collagen and supercritical fluids-assisted decellularized fibrous extracellular matrix. Polymers, 13: 4326.

   https://doi.org/10.3390/polym13244326

2. Tappa K, Jammalamadaka U, 2018, Novel biomaterials used in medical 3d printing techniques. *J Funct Biomater*, 9: 17.

   https://doi.org/10.3390/jfb9010017

3. Rhee S, Puetzer JL, Mason BN, *et al.*, 2016, 3D bioprinting of spatially heterogeneous collagen constructs for cartilage tissue engineering. *ACS Biomater Sci Eng*, 2: 1800–1805.

   https://doi.org/10.1021/acsbiomaterials.6b00288

4. Laronda MM, Rutz AL, Xiao S, *et al.*, 2017, A bioprosthetic ovary created using 3D printed microporous scaffolds restores ovarian function in sterilized mice. *Nat Commun*, 8: 15261.

   https://doi.org/10.1038/ncomms15261

5. Markstedt K, Mantas A, Tournier I, *et al.*, 2015, 3D bioprinting human chondrocytes with nanocellulose alginate bioink for cartilage tissue engineering applications. *Biomacromolecules*, 16: 1489–1496.

https://doi.org/10.1021/acs.biomac.5b00188

6. Nguyen D, Hägg DA, Forsman A, *et al*., 2017, Cartilage tissue engineering by the 3d bioprinting of ips cells in a nanocellulose/alginate bioink. *Sci Rep*, 7: 658.

7. Tan Z, Parisi C, Di Silvio L, *et al*., 2017, Cryogenic 3D printing of super soft hydrogels. *Sci Rep*, 7: 16293.

https://doi.org/10.1038/s41598-017-16668-9

8. Gao Q, Kim BS, Gao G, 2021, Advanced strategies for 3D bioprinting of tissue and organ analogs using alginate hydrogel bioinks. *Mar Drugs*, 19: 708.

https://doi.org/10.3390/md19120708

9. Chen YW, Hsieh DJ, Periasamy S, 2021, Development of a decellularized porcine bone graft by supercritical carbon dioxide extraction technology for bone regeneration. *J Tissue Eng Regen Med*, 15: 401–404.

https://doi.org/10.1002/term.3181

10. Seo Y, Jung Y, Kim SH, 2018, Decellularized heart ecm hydrogel using supercritical carbon dioxide for improved angiogenesis. *Acta Biomater*, 67: 270–281.

https://doi.org/10.1016/j.actbio.2017.11.046

11. Ma JZ, Hou XY, Gao DG, 2014, Greener approach to efficient leather soaking process: role of enzymes and their synergistic effect. *J Clean Prod*, 1: 226–232.

12. Kim BS, Kim JU, So KH, *et al*., 2021, Supercritical fluid-based decellularization technologies for regenerative medicine applications, *Macromol Biosc*, 21: e2100160.

https://doi.org/10.1002/mabi.202100160

13. Huang CC, Liu CY, Huang CY, *et al*., 2014, Carbodiimide cross-linked and biodegradation-controllable small intestinal submucosa sheets. *Biomed Mater Eng*, 24: 1959–1967.

https://doi.org/10.3233/BME-141005

14. Liu YW, Huang CC, Wang YY, *et al*., 2021, Biological evaluations of decellularized extracellular matrix collagen microparticles prepared based on plant enzymes and aqueous two-phase method. *Regen Biomater*, 8: rbab002.

https://doi.org/10.1093/rb/rbab002

15. Huang CC, 2022, Newly designed decellularized scaffolds for scaffold-based gene therapy from elastic cartilages via supercritical carbon dioxide fluid and alkaline/protease treatments. *Curr Gene Ther*, 22: 162–167.

https://doi.org/10.2174/1566523219666210618151843

16. Chou PR, Lin YN, Wu SH, *et al*., 2020, Supercritical carbon dioxide-decellularized porcine acellular dermal matrix combined with autologous adipose-derived stem cells: its role in accelerated diabetic wound healing. *Int J Med Sci*, 17: 354–367.

https://doi.org/10.7150/ijms.41155

17. Li Y, Xu Y, Liu Y, *et al*., 2019, Decellularized cartilage matrix scaffolds with laser-machined micropores for cartilage regeneration and articular cartilage repair. *Mater Sci Eng C Mater Biol Appl*, 105: 110139.

https://doi.org/10.1016/j.msec.2019.110139

18. Wang D, Zhu Y, Huang Y, *et al*., 2021, Pancreatic extracellular matrix/alginate hydrogels provide a supportive microenvironment for insulin-producing cells. *ACS Biomater Sci Eng*, 7: 3793–3805.

https://doi.org/10.1021/acsbiomaterials.1c00269

19. Hwang TI, Moon JY, Kim JI, *et al*., 2020, Fabrication of three-dimensional alginate porous scaffold incorporated with decellularized cornu cervi pantotrichum particle for bone tissue engineering. *J Nanosci Nanotechnol*, 20: 5356–5359.

https://doi.org/10.1166/jnn.2020.17676

20. Luo B, Loh QL, Chong MT, *et al*., 2014, Bioactivated protein-based porous microcarriers for tissue engineering applications. *J Mater Chem B*, 2: 7795–7803.

https://doi.org/10.1039/C4TB00846D

21. Zhang YS, Haghiashtiani G, Hübscher T, *et al*., 2021, 3D extrusion bioprinting. *Nat Rev Methods Primers*, 1: 75.

22. Lee JM, Yeong WY, 2020, Engineering macroscale cell alignment through coordinated toolpath design using support-assisted 3D bioprinting. *J R Soc Interface*, 17: 20200294.

https://doi.org/10.1098/rsif.2020.0294

23. Wang JK, Luo B, Guneta V, *et al*., 2017, Supercritical carbon dioxide extracted extracellular matrix material from adipose tissue. *Mat Sci Eng C Mater Biol Appl*, 75: 349–358.

https://doi.org/10.1016/j.msec.2017.02.002

24. Sun D, Liu Y, Wang H, 2018, Novel decellularized liver matrix-alginate hybrid gel beads for the 3D culture of hepatocellular carcinoma cells. *Int J Biol Macromol*, 109: 1154–1163.

https://doi.org/10.1016/j.ijbiomac.2017.11.103

25. Adochitei A, Drochioiu G, 2011, Rapid characterization of peptide secondary structure by ftir spectroscopy. *Rev Roum Chim*, 56: 783–791.

26. Chen K, Li J, Zhao W, *et al*., 2022, Physicochemical properties of collagen from the bone of *harpadon nehereus* and its protective effects against angiotensin ii-induced injury in human umbilical vein endothelial cells. *ACS Omega*, 7: 23412–23420.

https://doi.org/10.1021/acsomega.2c01739

27. Zhao WH, Chi CF, Zhao YQ, *et al*., 2018, Preparation, physicochemical and antioxidant properties of acid- and

pepsin-soluble collagens from the swim bladders of miiuy croaker (*Miichthys miiuy*). *Mar Drugs*, 16: 161.

https://doi.org/10.3390/md16050161

28. Nagai T, Izumi M, Ishii M, 2004, Fish scale collagen. Preparation and partial characterization. *Int J Food Sci Technol*, 39: 239–244.

https://doi.org/10.1111/j.1365-2621.2004.00777.x

29. Naghieh S, Karamooz-Ravari MR, Sarker MD, *et al*., 2018, Influence of crosslinking on the mechanical behavior of 3D printed alginate scaffolds: experimental and numerical approaches. *J Mech Behav Biomed Mater*, 80: 111–118.

https://doi.org/10.1016/j.jmbbm.2018.01.034